# Evaporation of solutions and colloidal dispersions in confined droplets

L. Daubersies and J.-B. Salmon
*Univ. Bordeaux, CNRS, Rhodia, LOF, UMR 5258, F-33680 Pessac, France*
(Received 8 July 2011; published 20 September 2011)

We present a model that describes the drying of solutions and colloidal dispersions from droplets confined between two circular plates. This confined geometry, proposed by Clément and Leng [Langmuir **20**, 6538 (2004)], casts a perfect control of the evaporation conditions, and thus also of the concentration kinetics of the solutes in the droplet. Our model, based on simple transport equations for binary mixtures, describes the concentration process of the solute inside the droplet. Using dimensionless units, we identify the different numbers that govern the concentration field of the solute, and we detail how to extract kinetic and thermodynamic information on the binary mixture from such drying experiments. We finally discuss, using numerical resolution of the model and analytical arguments, several specific cases: dilute solutions, a colloidal *hard sphere* dispersion, and a binary molecular mixture.

DOI: 10.1103/PhysRevE.84.031406 PACS number(s): 82.70.Dd

## I. INTRODUCTION

Evaporation of the solvent from a solution or a colloidal dispersion is a major *out-of-equilibrium route* for crossing dense phases starting from dilute states. Such a route is often explored thanks to the drying of a sessile droplet on a substrate [1]. Despite its apparent simplicity, such an experiment leads to a wide complexity (e.g., pinning of the contact line, divergence of the evaporation flux, thermal-induced Marangoni flows [2]), and a complete model describing the general case of the drying of mixtures up to dense states is missing. Moreover, tuning the kinetics of evaporation is often a challenge in such experiments. To overcome these difficulties, several groups proposed *confined* geometries for (1) bringing a kinetic control on the evaporation conditions and (2) being able to develop simple models to describe the evaporation process from dilute up to dense mixtures. Among the strategies proposed, one can cite the solidification of dispersions or polymer solutions confined between parallel plates as thin liquid films [3–5] (see also the review [6] for polymer solutions), or even continuous evaporation in nanoliter chambers using microfluidics [7,8].

Following a similar strategy, Clément and Leng proposed and investigated the drying of droplets squashed between two circular plates (see Fig. 1) [9]. Typically, droplets with volumes ranging from 0.5 to 2 $\mu$L adopt a *pancake* shape with radii $R_i \approx 1$–4 mm when confined between wafers separated by spacers $h \approx 50$–$100\mu$m. This axis-symmetrical confined geometry allows a neat control of the vapor removal from the edge of the droplet $R_i$ toward the edge of the wafer $R_w$ and therefore provides a simple way to tune the drying kinetics by changing the size of the circular plates. Moreover, this two-dimensional (2D) geometry leads to an easy observation of the drying process, and wettability of the circular plates can be changed due to appropriate coatings deposited using standard spin-coating processes.

Clément and Leng investigated the evaporation of pure liquids in such a geometry and demonstrated that the temporal evolution of the droplet area $A(t)$ gives access to the gas diffusivity of the solvent molecules in air [9]. Importantly, they also showed that the evaporation kinetics is modified in the case of molecular solutions, such as salty water, and that a precise monitoring of $A(t)$ leads to the determination of the activity of the mixture. More recently, Leng investigated the drying of colloidal hard sphere (HS) dispersions using the same geometry [10]. In this case, drying leads to the formation of a dense *crust* at the edge of the drop. This shell then invades the droplet as drying continues and ultimately induces a buckling instability. Similar experiments were also performed by Pauchard *et al*. to investigate specifically this instability [11]. The observed phenomenology for such colloidal dispersions differs strongly from the drying of molecular mixtures, as the diffusive transport of the solutes (colloids vs molecules) is different.

The aim of the present work is to provide a simple model based on classical transport equations for binary mixtures that can describe the drying kinetics $A(t)$ and the concentration field of solute $\phi(R,t)$. Such a model should describe the evaporation of the solvent from binary mixtures such as colloidal dispersions, polymer solutions, or molecular solutions, for which the solute is supposed to be nonvolatile. In the following, we assume several hypotheses to derive a simple model whose resolution does not require complex numerical techniques. We also show how experimental measurements of the evolution of the droplet area $A(t)$ and of the concentration field of solute $\phi(R,t)$, confronted with numerical resolution of the model, should provide kinetic and thermodynamic information on the binary mixture (activity and mutual diffusion coefficient; see Sec. II C).

We then discuss several cases that are often explored experimentally: dilute solutions, a HS colloidal dispersion, and a molecular mixture. In the first case, we provide an analytical formula that describes correctly the concentration field of solute. For the colloidal dispersion, our model captures the formation of a dense crust that invades the inner of the droplet during drying. Finally, we illustrate the case of molecular solutions using numerics in the case of water-glycerol mixtures for which the evolution of the transport properties with the solute concentration (mutual diffusion coefficient), as well as the activity of the mixture, are well known.

 

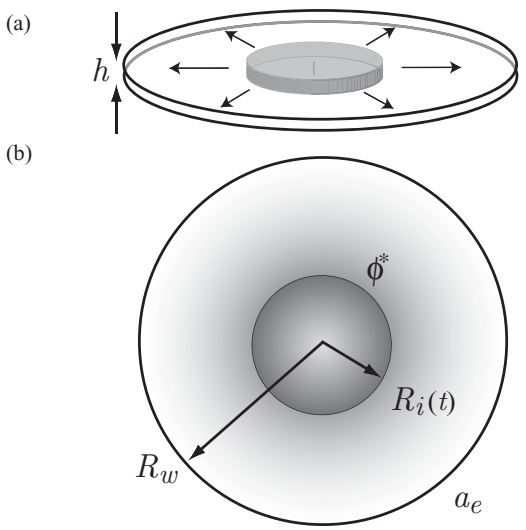


FIG. 1. (a) Three-dimensional view of the geometry of the confined droplet squashed between two circular plates separated by a distance $h$. (b) Top view: $R_i(t)$ is the droplet radius, $R_w$ that of the plates, $a_e$ the external *humidity* condition, and $\phi^\star$ the concentration at the interface. The gray scale illustrates the concentration gradients of solute inside the droplet, and of the solvent in the vapor phase.

## II. A SIMPLE MODEL FOR THE DRYING OF CONFINED DROPLETS

### A. Transport equations and boundary conditions

We first consider a typical experiment as described in Fig. 1. A droplet of a solution (or a dispersion) is confined between two parallel and circular wafers of radius $R_w$. In the following, we consider binary mixtures only, with a volatile solvent and a nonvolatile solute that does not present any specific interactions with the wafers. The droplet keeps a circular shape during the evaporation of the solvent, due to its surface tension, and also because we assume there are no pinning of the contact line (this is indeed observed experimentally as soon as wafers with appropriate coatings are used [12]). Moreover, confinement ($h \ll R_i$) also minimizes effects of contact line hysteresis (as compared to the case of sessile droplets) because receding values of the contact angle are rapidly reached upon evaporation (the *volume of the meniscus* $\sim R_i h^2$ is small compared to the droplet's one $\sim R_i^2 h$). We also suppose that diffusion homogeneizes the concentration fields in the droplet and in the vapor phase along the $z$ direction, leading to a simple one-dimensional (1D) axis-symmetrical description. This situation is easily obtained when the height $h$ separating the wafers is small compared to the other dimensions.

Inportantly, we restrict our model to *quiescent* and *isothermal* droplets during drying. This may be a strong limitation since Rayleigh-Bénard-Marangoni (thermal or solutal) instabilities that induce recirculation flows are often observed in similar drying experiments (see, for instance, Refs. [13,14] for sessile droplets, Ref. [15] for three-dimensional droplets, and Ref. [16] for evaporation from thin films, and references therein). Thermal gradients coming from evaporation are generally small in the case of slightly volative solvents (e.g., $<0.01$ K for water in a sessile droplet; see Ref. [14]), and they have probably no significant effects on the transport properties of the mixture considered (isothermal droplet), but often induce Marangoni recirculation flows [13,14]. However, in the confined geometry considered here, such instabilities have only been observed in the case of water-surfactant solutions [17], but not for colloidal dispersions [10] and for several other aqueous solutions [12]. These results point to the fact that the observed instabilities probably arise from solutal gradients and unveil the role of confinement to prevent thermal Marangoni flows, as noted by Leng in Ref. [10]. An experimental and theoretical analysis of such instabilities in this specific geometry is left for a future work, and we assume in the following a quiescent and isothermal droplet during drying.

#### 1. Transport equations in the vapor phase

We define $c_S$ the molar concentration of solvent in the vapor state, $c_a$ that of air, $x_S$ and $x_a$ their corresponding molar fractions. We assume, as done usually, perfect gas conditions, i.e., $c_S + c_a = c = \text{const}$. The molar solvent flux takes the classical form [18–20]:

$$\boldsymbol{n}_S = c_S \boldsymbol{v}_m - \tilde{D} c \boldsymbol{\nabla} x_S, \tag{1}$$

where $\tilde{D}$ is the diffusion coefficient of the solvent in the vapor phase, and $\boldsymbol{v}_m$ the molar-averaged velocity defined by

$$c\boldsymbol{v}_m = \boldsymbol{n}_a + \boldsymbol{n}_S, \tag{2}$$

where $\boldsymbol{n}_a$ is the molar air flux in the gas phase.

#### 2. Transport equation in the liquid phase

We consider a binary mixture composed of a volatile solvent and a nonvolatile solute, and we restrict our analysis to the case of a simple mixture; i.e., both constituents of the mixture are incompressible. The volume-averaged velocity $\boldsymbol{v}_v$ is defined as [18–20]

$$\boldsymbol{v}_v = \boldsymbol{j} + \boldsymbol{j}_S, \tag{3}$$

where $\boldsymbol{j}$ and $\boldsymbol{j}_S$ are the solute and solvent volumic fluxes. For the case of a simple mixture, the mass density is a linear function of the solute volume fraction $\phi$, and the volume-averaged velocity obeys $\text{div}\boldsymbol{v}_v = 0$ [21]. For a quiescent droplet one has thus $\boldsymbol{v}_v = \boldsymbol{0}$, and the volumic flux of solute is [18–20]

$$\boldsymbol{j} = -\boldsymbol{j}_S = -D(\phi)\boldsymbol{\nabla}\phi, \tag{4}$$

where $D(\phi)$ is the mutual diffusion coefficient of the mixture in the reference frame of the volume-averaged velocity (also called *long-time collective* or *gradient* diffusion coefficient in the context of colloidal dispersions). The conservation of the solute in the droplet leads to

$$\partial_t \phi = \text{div}[D(\phi)\boldsymbol{\nabla}\phi]. \tag{5}$$

The mutual diffusion coefficient $D(\phi)$ is intimately related to bulk thermodynamic and kinetic properties of the mixture. In the case of a colloidal dispersion, for instance, $D(\phi)$ strongly depends on the interactions (through the osmotic compressibility), but also on the hydrodynamic interactions [22,23] (see Sec. III B).

#### 3. Boundary conditions

The jump mass balance at the liquid-gas interface moving at a velocity $\dot{R}_i$ leads to the conditions [24]

$$n_a^\star = c_a^\star \dot{R}_i, \tag{6}$$

$$j^\star = \phi^\star \dot{R}_i, \tag{7}$$

$$j_S^\star - (1-\phi^\star)\dot{R}_i = \nu_S(n_S^\star - c_S^\star \dot{R}_i), \tag{8}$$

where $\nu_S$ is the molar volume of the solvent in the liquid state, and the symbol $\star$ indicates values taken at the interface $R = R_i(t)$. From the above conditions, the velocity of the interface is related to the flux of solvent in the gas phase:

$$\dot{R}_i = \frac{\nu_S}{\nu_S c_S^\star - 1} n_S^\star. \tag{9}$$

Finally, we assume a constant humidity at the edge of the wafer, so that $x_S(R_w) = x_S^w$ is imposed (we use here the term *humidity* to denote the concentration of the solvent in air, even if the later is not water).

### B. Quasistationary approximation: Evolution of the droplet area

We now suppose that the droplet evaporation is very slow compared to the transport in the vapor phase (only slightly volatile solvents are thus considered $x_S^\star \ll 1$). Concentrations in the gas phase thus quickly reach a steady state, on a time scale given by $R_w^2/\tilde{D}$, and the air and solvent fluxes verify $\mathrm{div}\boldsymbol{n}_a = \mathrm{div}\boldsymbol{n}_S = 0$. The above mass balance conditions lead to

$$Rn_a = R_i(c - c_S^\star)\dot{R}_i. \tag{10}$$

According to Eq. (1), the solvent flux in the vapor phase is now

$$n_S = cx_S \frac{1-x_S^\star}{1-x_S}\frac{R_i\dot{R}_i}{R} - \tilde{D}c\frac{\partial_R x_S}{1-x_S} \approx -\tilde{D}c\frac{\partial_R x_S}{1-x_S}, \tag{11}$$

since $\dot{R}_i \ll \tilde{D}/R_i$ (quasistationary approximation). Finally, the flux of solvent in the gas phase can be calculated from the integration of the above equation using the boundary conditions at $R_i(t)$ and $R_w$:

$$n_S = \frac{-\tilde{D}c}{R\ln(R_i/R_w)}\ln\left(\frac{1-x_S^w}{1-x_S^\star}\right).$$

The mass balance at the interface [see Eq. (9)] leads now to the droplet evolution:

$$\dot{R}_i = \frac{\nu_S}{\nu_S c_S^\star - 1}\frac{-\tilde{D}c}{R_i\ln(R_i/R_w)}\ln\left(\frac{1-x_S^w}{1-x_S^\star}\right), \tag{12}$$

which depends explicitly on the molar concentration $x_S^\star$ of solvent molecules at the interface. This last equation is an equivalent in a 2D geometry of the classical problem of evaporation in a column (often called the *Stefan* tube [18–20]).

For simplicity (without loss of generality), we consider slightly volatile solvents ($x_S^\star \ll 1$), and for which there is a large difference between the densities of the vapor and of the liquid state, i.e., $\nu_S c_S^\star \ll 1$ ($x_S^\star \approx 0.03$ and $\nu_S c_S^\star \approx 10^{-5}$ for pure water at room temperature). The droplet evolution during evaporation thus takes the simpler form:

$$\dot{R}_i \approx \frac{\nu_S\tilde{D}\left(c_S^\star - c_S^w\right)}{R_i\ln(R_i/R_w)} = \frac{\nu_S\tilde{D}c_S^{\mathrm{sat}}(a(\phi^\star) - a_e)}{R_i\ln(R_i/R_w)}, \tag{13}$$

where $c_S^{\mathrm{sat}}$ is the molar concentration at saturation of the pure solvent in the gas phase, $a(\phi^\star)$ the activity of the mixture at the interface, and $a_e = c_S^w/c_S^{\mathrm{sat}}$ the relative humidity at the edge of the wafer. This last equation is now similar to the one derived by Clément and Leng [9] on the basis of a purely diffusive transport in the gas phase, but with the important following difference: The evolution of $R_i(t)$ depends now on the activity of the mixture at the *interface*, i.e., at the concentration $\phi^\star$.

This last equation also shows that the drying kinetics of the droplet roughly scales as $R_0^2/\nu_S\tilde{D}c_S^{\mathrm{sat}}$ [see Eq. (24) later in the text for the prefactors in the case of a dilute solution or dispersion]. The quasistationary approximation is therefore valid when the transport in the gas phase (on a time scale $R_w^2/\tilde{D}$) is faster than the drying kinetics, i.e., for $\nu_S c_S^{\mathrm{sat}} \ll (R_0/R_w)^2$.

### C. Final model: Link to thermodynamic and kinetic properties of the mixture

The final model and the boundary condition (7) now read

$$\dot{R}_i = \frac{\nu_S\tilde{D}c_S^{\mathrm{sat}}[a(\phi^\star) - a_e]}{R_i\ln(R_i/R_w)}, \tag{14}$$

$$\partial_t\phi = \mathrm{div}(D(\phi)\nabla\phi), \tag{15}$$

$$-D(\phi^\star)\partial_R\phi^\star = \phi^\star\dot{R}_i. \tag{16}$$

An experiment measuring precisely the concentration field of solute $\phi(R,t)$, and the evolution of the droplet radius $R_i(t)$ during drying, should *a priori* lead to estimations of both activity $a(\phi)$ and mutual diffusion coefficient $D(\phi)$, i.e., thermodynamic and kinetic properties of the mixture. In this sense, such an experiment is similar to other out-of-equilibrium routes such as sedimentation, ultrafiltration, or microevaporation [25,26], but with a facilitated observation, and for solutes ranging from molecules to colloids.

### D. Dimensionless model

We define the following dimensionless variables:

$$r = R/R_0, \quad \alpha = (R_i(t)/R_0)^2, \quad \beta = (R_0/R_w)^2,$$
$$\tau = t/\tau_d, \hat{D}(\phi) = D(\phi)/D_0,$$

with

$$\tau_d = R_w^2/\left(4\nu_S c_S^{\mathrm{sat}}\tilde{D}\right),$$

and where $R_0$ is the initial radius of the droplet and $D_0$ the diffusion coefficient at zero concentration [i.e., $\hat{D}(0) = 1$]. $\tau_d$ is the natural time scale of the evaporation process that can be tuned by the area of the wafers $R_w^2$. With such dimensionless coordinates, the initial condition for the dimensionless area of the droplet $\alpha$ is $\alpha(\tau = 0) = 1$. We also define the following parameter:

$$\mathrm{Pe} = R_0^2/(D_0\tau_d) = \beta\frac{4\nu_S c_S^{\mathrm{sat}}\tilde{D}}{D_0},$$

which is similar to a Péclet number, since it compares the typical distance explored by diffusion $D_0\tau_d$ during drying, over the area of the droplet $R_0^2$.

The evolutions of $\alpha$, of the solute concentration $\phi$, and of the boundary condition can now be written

$$\frac{d\alpha}{d\tau} = \frac{a(\phi^\star) - a_e}{\beta \ln(\alpha\beta)}, \tag{17}$$

$$\partial_\tau \phi = \frac{1}{r}\partial_r \left[ r \frac{\hat{D}(\phi)}{\mathrm{Pe}} \partial_r \phi \right] \quad \text{for} \quad r < \sqrt{\alpha} \tag{18}$$

$$\frac{a(\phi^\star) - a_e}{2\sqrt{\alpha}\beta \ln(\beta\alpha)} = -\frac{\hat{D}(\phi^\star)}{\mathrm{Pe}} \frac{\partial_r \phi^\star}{\phi_\star} \quad \text{at} \quad r = \sqrt{\alpha}. \tag{19}$$

This model involves only three parameters, $a_e$, Pe, and $\beta$, that can be tuned experimentally due to the ratio $R_0/R_w$ and the external humidity conditions (kinetic control). The model compared to experimental results should provide estimations of $a(\phi)$ (thermodynamics) and $\hat{D}(\phi)$ (kinetics).

### E. Numerical resolution

To solve numerically the above problem, we need a fixed interval for the space coordinate. We thus apply the change of coordinates $\phi(r,t) \to \phi(u,t)$, with $r = \sqrt{\alpha}u$, and $u$ ranging from 0 to 1. This coordinate transformation adds an advection-like term to the evolution equation, and the above equations now take the simple form

$$\frac{d\alpha}{d\tau} = \frac{a(\phi^\star) - a_e}{\beta \ln(\alpha\beta)}, \tag{20}$$

$$\partial_\tau(\alpha\phi) = \frac{1}{u}\partial_u[uJ(u)], \tag{21}$$

$$J(u) = \frac{\hat{D}(\phi)}{\mathrm{Pe}}\partial_u\phi + \frac{u\phi}{2}\frac{d\alpha}{d\tau}, \quad J(u=1) = 0.t \tag{22}$$

Such a model can be solved easily using a standard discretization of the space coordinate $u$, and the classical fourth-order Runge-Kutta numerical scheme [27].

## III. SOLUTIONS AND COLLOIDAL DISPERSIONS

In this section we discuss several limiting cases, dilute solutions (or dispersions), a HS colloidal dispersion, and finally the case of a molecular mixture (glycerol and water). For all the investigated cases, our aim is to illustrate using numerics and/or analytical arguments the process of solute concentration in the droplet during evaporation.

### A. Dilute solutions and dispersions

#### 1. *Influence of the* Pe *number on the concentration process*

We first consider dilute solutions or dispersions for which $a(\phi) = 1$ and $\hat{D}(\phi) = 1$. We also assume $a_e = 0$ for more simplicity without any loss of generality since one can define a new time scale of drying in the dilute case, according to $\tau_d \to (1 - a_e)\tau_d$. The model thus now only depends on two parameters: $\beta$ and the Péclet number Pe. In this regime, the evolution of the droplet area $\alpha$ does not depend anymore on the solute concentration and is simply given by integration of Eq. (20):

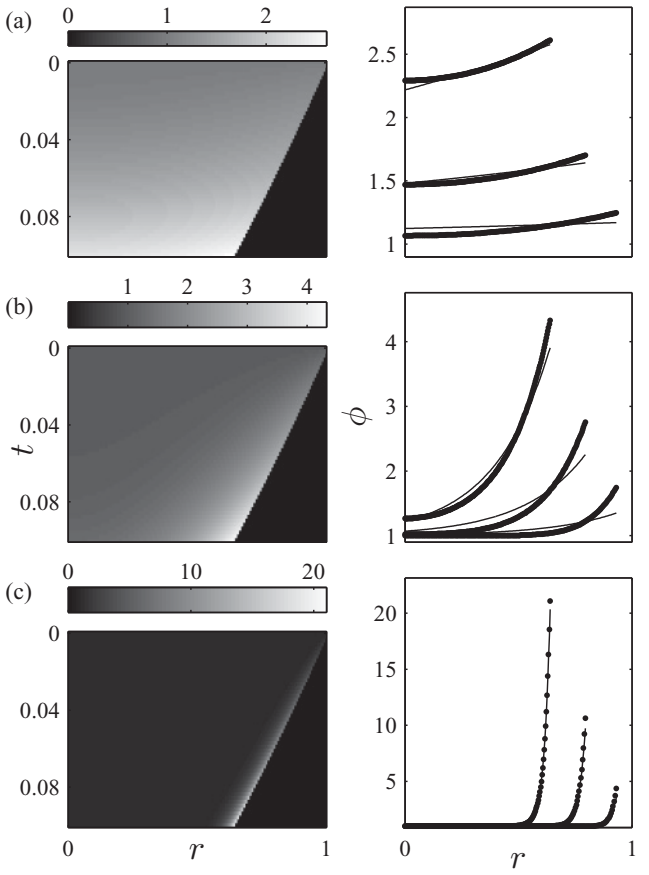


FIG. 2. Dilute case, $\hat{D} = 1$, $a = 1$, $\beta = 0.05$ but for different Péclet numbers Pe = 0.1 (a), 1(b), and 10(c). Left: space-time plots of the concentration fields $\phi(r,t)$. Right: Typical concentration profiles at $t = 0.02$, 0.06, and 0.1. The continuous lines are the theoretical estimations given by Eq. (25).

$$\tau = \beta\alpha[\ln(\beta\alpha) - 1] - \beta[\ln(\beta) - 1]. \tag{23}$$

Complete drying of the droplet occurs at time $\tau_f = \beta[1 - \ln(\beta)]$. Using dimensionalized units, complete drying thus occurs for

$$t_f = \frac{R_0^2}{4\nu_S \tilde{D} c_S^{\mathrm{sat}}}(1 - \ln\beta); \tag{24}$$

at a fixed initial radius of droplet $R_0$, one can control the drying kinetics through the ratio $\beta = (R_0/R_w)^2$.

Figure 2 displays numerical results of the concentration field during evaporation obtained for $\beta = 0.05$ but for different Péclet numbers Pe = 0.1 (a), 1(b), and 10(c). $\mathrm{Pe} = R_0^2/(D_0\tau_d)$ compares the diffusion time over the droplet $R_0^2/D_0$ and the kinetics of drying $\tau_d$. For low Pe numbers, one thus expects that diffusion is faster than evaporation, and thus homogeneous concentration fields, as demonstrated in Fig. 2(a). For higher Péclet numbers (Pe > 1), significant concentration gradients build up during drying close to the droplet edge [see Figs. 2(b)–2(c)], as the drying kinetics is now faster than the diffusion of solutes.

#### 2. *High* Pe *regime: An analogy with filtration*

In the case of high Péclet numbers (Pe $>$ 10), the extension of the concentration gradients is strongly localized at the droplet meniscus, and thus smaller than the droplet radius. In this regime the curvature of the droplet can be neglected, and one can identify the concentration process of the solute, from the reference frame of the meniscus, as the *filtration* of solutes through a *membrane* at a *flow rate* given by the meniscus velocity.

In the case of one-dimensional filtration of dilute solutes through a membrane (along the $x$ direction), the flux of solutes is given by $j(x) = v\phi - D_0\partial_x\phi$ and vanishes at the membrane position ($x = 0$). In the asymptotic regime, i.e., for a constant flux, $j(x)$ is proportional to $j(x) \sim 1 - \exp(-x/\xi)$ where $\xi = D_0/v$ is the natural length scale balancing diffusion and convection. In this asymptotic regime, the solute concentration increases linearly with time and is approximatively proportional to $\phi \propto \exp(-x/\xi)t$. By analogy with this simple filtration problem, we propose a similar approximation for the concentration field in the high Péclet regime:

$$\phi(r,t) \approx 1 + A(t)\exp\left(\frac{r-\sqrt{\alpha}}{\xi}\right), \tag{25}$$

where $\xi$ is the length scale that comes from the competition between convection and diffusion, which is written with our dimensionless units in the case of the confined droplet:

$$\xi = -\frac{2\sqrt{\alpha}}{\mathrm{Pe}}\beta\ln\alpha\beta.$$

The evolution of $A(t)$ can be calculated analytically from the conservation of the solute in the droplet during evaporation:

$$2\int_0^{\sqrt{\alpha}} dr r\phi(r,t) = 1. \tag{26}$$

This analytical estimation of the concentration field is plotted in Fig. 2 for the different investigated Péclet numbers. For Pe $>$ 10, Eq. (25) gives a good approximation of the concentration field as expected, since the extension of the concentration gradients is small compared to the droplet radius. Interestingly, the same formula gives rather good approximations of $\phi(r,t)$ for small Pe numbers and thus may serve as a guide without a numerical resolution of the problem.

### B. Hard sphere colloidal suspensions

#### 1. *Observed phenomenology for hard sphere suspensions*

We now turn to colloidal dispersions, and more precisely to HS dispersions, for which there are only entropic colloidal interactions [22]. Leng investigated recently [10] the drying of confined droplets (Fig. 1) of a well-known colloidal system that presents HS interactions in decalin [28]. During the slow evaporation of decalin from the droplet, Leng observed the following scenario. The droplet first starts receding as a consequence of decalin removal. Then, a front separating a dense *crust* and a dilute dispersion starts to invade the inner of the droplet from its edge. Finally, droplets do not keep their circular shape during the complete drying process as a buckling instability occurs leading to complex morphologies (*invagination* [11], fracture, etc.). Interestingly, a careful analysis reveals that the crust corresponds to either amorphous deposits of colloids or well-organized crystallites, depending on the experimental conditions (e.g., size of the colloids). Note that formation of crusts upon drying is ubiquitous as soon as drying is used to promote self-assembly of colloids or nanoparticles (in the case of sessile droplets, for instance, even leading to perfectly ordered monolayers [29]). It is clear that our simple model cannot reproduce the rich complexity of these observations; however, we illustrate below how it can predict the formation of the crust and its growth during drying.

#### 2. *A model for $a(\phi)$ and $\hat{D}(\phi)$ in the case of hard sphere dispersions*

First, the experimental conditions investigated in Ref. [10] are close to the approximations done to derive our model (slow evaporation of the solvent, binary and simple mixture, etc.). We can thus safely use Eqs. (20)–(22) to describe the concentration process, at least before the observed instabilities (i.e., when the suspension does not present *solid* properties).

Second, colloidal interactions in a HS dispersion hardly affect the evaporation rate, and the activity of the solvent is $a(\phi) \approx 1$. Indeed, $a(\phi)$ follows

$$a(\phi) = \exp\left[-\frac{v_m}{v_c}\phi Z(\phi)\right], \tag{27}$$

where $v_c$ is the volume of the colloids, $v_m$ that of the solvent molecules, and $Z(\phi)$ the osmotic compressibility of the colloidal dispersion [22]. Due to the huge difference between $v_c$ and $v_m$ ($v_m/v_c \approx 5\,10^{-9}$ for decalin and colloids of radius 230 nm), the colloidal assembly does not alter significantly $a(\phi)$, and thus the evaporation rate [30].

Finally, as HS dispersions are well documented in the literature, one can find numerous measurements as well as theoretical calculations for $Z(\phi)$, and for the sedimentation coefficient $K(\phi)$, that describes hydrodynamic interactions at finite concentration $\phi$ [22]. These two quantities lead to an estimate of the long-time collective coefficient diffusion $D(\phi)$ due to the generalized Stokes-Einstein equation [22,31]:

$$D(\phi) = D_0K(\phi)\frac{d\phi Z(\phi)}{d\phi}, \tag{28}$$

where $D_0$ corresponds to the diffusion coefficient in the dilute limit.

To estimate $D(\phi)$, we consider here for simplicity that the HS dispersion does not crystallize upon concentration but becomes glassy around $\phi_g \approx 0.64$, the random-close packing fraction. Indeed, nucleation and growth of colloidal crystallites may not occur during evaporation of the droplet, due to the competition between the nucleation kinetics and that of the solute concentration [32]. This was observed experimentally for large colloids in the confined droplet [10], but also for polydisperse dispersions in several other experiments. We can now use an analytical formula derived by Peppin *et al.* for $Z(\phi)$ [see Eq. (2.17) in Ref. [33]]:

$$Z(\phi) = \frac{1 + a_1\phi + a_2\phi^2 + a_3\phi^3 + a_4\phi^4}{1 - \phi/\phi_g},$$

with $a_1 = 4 - 1/\phi_g$, $a_2 = 10 - 4/\phi_g$, $a_3 = 18 - 10/\phi_g$, and $a_4 = 1.85/\phi_g^5 - 18/\phi_g$. This formula approximates the

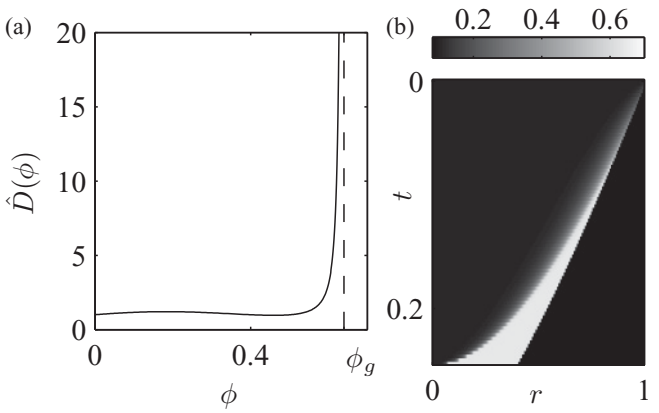


FIG. 3. (a) Collective diffusion coefficient $\hat{D}(\phi)$ for a HS dispersion according to Ref. [33]. $\hat{D}(\phi)$ diverges approaching the random-close packing fraction at $\phi_g \approx 0.64$. (b) Space-time plot of the concentration field $\phi(r,t)$ obtained by numerical resolution of Eqs. (20)–(22) in the case Pe = 10, $\beta = 0.1$, $\phi_0 = 0.1$ (these values are close to those investigated in Ref. [10]).

classical Carnahan-Starling equation at low $\phi$ and matches the divergence of $Z(\phi)$ approaching $\phi_g$ according to $Z(\phi) = 1.85/(\phi - \phi_g)$ [22,34,35]. For the sedimentation factor $K(\phi)$, we tested several formulas (experimental data [36,37], or theoretical estimations from the permeability of randomly packed monodisperse spheres [38]) that all give similar results, and we use in the following the same law used by Peppin *et al.*, i.e., $K(\phi) = (1 - \phi)^6$.

Figure 3(a) displays $\hat{D}(\phi) = D(\phi)/D_0$ calculated from Eq. (28) due to the above estimations of $Z(\phi)$ and $K(\phi)$. As already mentioned by Russel *et al.* [22], the collective diffusion coefficient shows a weak dependence on the volume fraction for $\phi < \phi_g$, as the hydrodynamic interactions almost cancel the increase of osmotic compressibility. However, $\hat{D}(\phi)$ rapidly diverges around $\phi_g$ as the colloidal assembly cannot be packed anymore (divergence of the osmotic compressibility) but still presents a finite permeability (solvent can flow through the close-packed assembly).

### 3. Concentration process and growth of a dense crust

Figures 3(b) and 4 display a numerical resolution of Eqs. (20)–(22) using $a(\phi) = 1$, and the collective diffusion coefficient $\hat{D}(\phi)$ displayed in Fig. 3(a). We chose to illustrate the experiments done by Leng, using a droplet of a HS colloidal dispersion at an initial volume fraction $\phi = 0.1$, with $\beta = 0.1$ and Pe = 10, these values being close to those investigated in Ref. [10]. We also consider that there is no decalin vapor in air, and thus $a_e = 0$.

As shown in Fig. 4, the model reproduces quantitatively the observed phenomenology [10]. At early times, the concentration of colloids increases at the edge of the droplet, up to the maximal packing fraction $\phi_g$. At later times, a shell corresponding roughly to $\phi \approx \phi_g$ invades the inner of the droplet as the droplet still recedes (see Fig. 4, bottom). As mentioned above, the collective diffusion coefficient $D(\phi)$ displays a weak dependence with volume fraction below $\phi_g$. This is again confirmed in Fig. 4 (top), where we plotted the estimations of the concentration profiles given by Eq. (25),

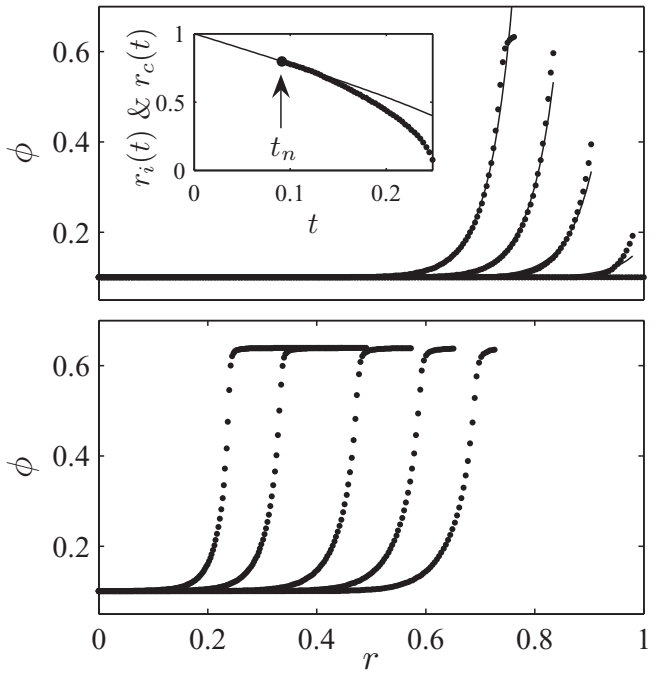


FIG. 4. The case of a HS dispersion for the parameters Pe = 10, $\beta = 0.1, \phi_0 = 0.1$. Concentration profiles corresponding to the space-time plot displayed in Fig. 3. Top: Times $t$ before the growth of a *crust* at $\phi \approx \phi_g$. The continuous lines are the theoretical estimations given by Eq. (25) (see text). Bottom: Later times $t > t_n$. Inset: Position of the front of the crust $r_c(t)$ (dots), and of the droplet radius $r_i(t)$ (continuous line). The arrow indicates the time $t_n$ at which the dense shell invades the inner droplet estimated using Eq. (25) (see text).

i.e. for a dilute dispersion, and thus for a *constant* diffusion coefficient. The agreement between the estimations and the numerical resolution of the model thus confirms that the colloidal assembly behaves roughly as a dilute suspension below the random-close packing fraction.

For later times, as the osmotic compressibility and thus $D(\phi)$ diverge, a *front* separating a dilute suspension and a *dense crust* invades the inner of the droplet for $t > t_n \approx 0.09$. The position $r_c(t)$ of that crust is plotted against time $t$ in the inset of Fig. 4. We estimate $r_c(t)$ at the positions $r$ given by $\phi(r,t) = 0.635$, but other values in the range 0.62–0.64 give similar results, because $D(\phi)$ strongly diverges at $\phi \approx \phi_g$. As evidenced in this plot, $r_c(t)$ rapidly deviates from the meniscus position $r_i(t) = \sqrt{\alpha(t)}$, and its velocity increases at longer time scales. The estimation of the concentration profiles given by Eq. (25) for a dilute dispersion also permits us to estimate analytically $t_n$, the time at which $\phi$ reaches $\phi_g$ at the droplet interface. This estimation is in clear agreement with the data displayed in the inset of Fig. 4.

Finally, Fig. 4 evidences concentration gradients in front of the dense shell for $t > t_n$. As the crust invades the inner of the droplet, the gradients of concentration become stiffer, since the velocity of $r_c(t)$ increases with time. A detailed theoretical study, such as done in Ref. [39] in a similar context (evaporation from films containing colloidal dispersions), should *a priori* provide analytical formulas to describe precisely the concentration profiles close to the front.

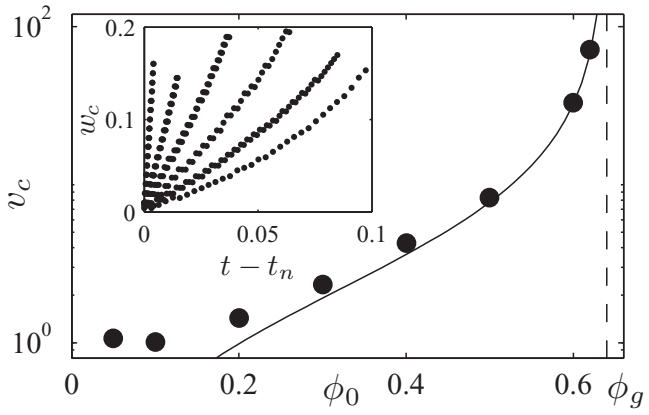


FIG. 5. Growth velocity of the crust $v_c$ vs $\phi_0$. The parameters of the simulations are Pe = 10 and $\beta = 0.1$; $v_c$ is defined as the initial slope of the width of the crust $w_c(t)$; $w_c$ are displayed against $t - t_n$ in the inset for various $\phi_0$ in the range 0.1–0.6. The continuous line is the approximation of $v_c$ given by Eq. (30).

#### 4. Crust velocity growth

We can also estimate from our simulations the width $w_c$ of the crust as a function of time, defined by $w_c = r_i - r_c$ (see Fig. 4). The inset of Fig. 5 displays $w_c$ as a function of time $t$, for several initial conditions $\phi_0$ in the drying droplet. For all these numerical simulations, Pe = 10 and $\beta = 0.1$ as before, and we subtracted the *nucleation* times $t_n$ to compare the different curves. Here $w_c$ increases linearly with time at early stages and then speeds up, at least for the small $\phi_0$. We define the growth velocity of the crust $v_c$ as the initial slope of $w_c(t)$, as done experimentally by Leng in Ref. [10]. Figure 5 displays $v_c$ as a function of $\phi_0$, the initial volume fraction in the droplet. As shown on this plot, $v_c$ diverges approaching the random-close packing fraction $\phi_g$. This was also observed experimentally by Leng [10], and explained in terms of a *truncated dynamics* by analogy with a similar problem in the context of deposit formation in evaporating sessile droplets [40]. For large Pe numbers, the extension of the gradients of concentration in front of the crust can be neglected, and the droplet is *divided* in two domains: $\phi = \phi_0$ for $r < r_c(t)$ and a *deposit* at $\phi \approx \phi_g$ for $r > r_c(t)$. Within this approximation, mass conservation of the solute then leads to

$$v_c = -\dot{r_i}\frac{\phi_0}{\phi_g - \phi_0}\left(1 + \frac{\phi_g w_c}{\phi_0 r_c}\right) \approx -\dot{r_i}\frac{\phi_0}{\phi_g - \phi_0}, \quad (29)$$

the last approximation being valid for early times, when the width of the crust verifies $w_c/r_c \ll \phi_0/\phi_g$. A simple estimate of $\dot{r_i}$ can be given for $t \approx 0$ using the droplet evolution equation [see Eq. (20)], and the velocity of the growth of the crust finally follows at early times:

$$v_c \approx \frac{-1}{2\beta \ln(\beta)}\frac{\phi_0}{\phi_g - \phi_0}. \quad (30)$$

This last relation is plotted in Fig. 5 and accounts well for the data at high $\phi_0$, as also demonstrated experimentally in Ref. [10]. Indeed, nucleation times $t_n$ are small at high initial volume fractions $\phi_0$, and the condition $w_c/r_c \ll \phi_0/\phi_g$ is easily satisfied. However, $v_c$ versus $\phi_0$ deviates from the above approximation at smaller $\phi_0$. This is first due to the fact that $r_i(t)$ cannot be approximated at $t \approx 0$ since the formation of the crust occurs at longer time, but also because $w_c\phi_g/(r_c\phi_0)$ cannot be neglected anymore. Note that this regime of small $\phi_0$ (<0.2) was not explored by Leng in Ref. [10].

### C. Solutions: The case of a water-glycerol mixture

We finally turn to the case of a solution, for which both the activity and the mutual diffusion coefficient vary with the concentration $\phi$. Such a situation is often encountered for molecular mixtures or polymers in solution. We decide to illustrate this case with water-glycerol solutions, first, because it corresponds to a simple binary mixture, but also because thermodynamic $a(\phi)$ and kinetic properties $D(\phi)$ can be found in the literature.

#### 1. Activity $a(\phi)$ and collective diffusion coefficient $D(\phi)$

Figure 6(a) displays the density $\rho$ of such mixtures against the volume fraction of glycerol $\phi$ [41]. Here $\rho(\phi)$ is very well approximated by $\rho(\phi) = \rho_g\phi + (1-\phi)\rho_w$, with $\rho_g$ and $\rho_w$ the densities of pure glycerol and pure water, respectively, and this indicates a simple mixture; i.e., both constituents are incompressible upon mixing [21]. Figures 6(b) and 6(c) display the activity $a(\phi)$ as well as the mutual diffusion coefficient $D(\phi)$ computed from several measurements found in the literature [42–47]. Data for $D(\phi)$ are rather dispersed

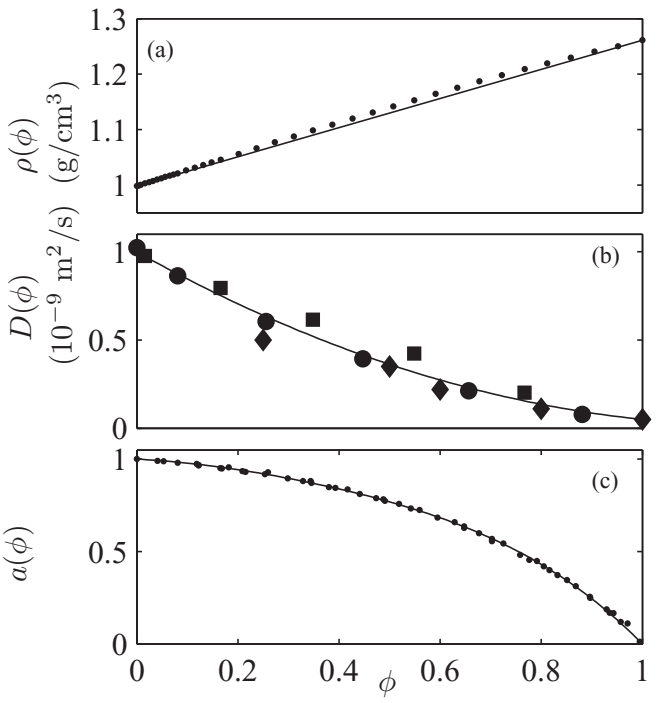


FIG. 6. Properties of water-glycerol mixtures vs glycerol volume fraction $\phi$ at $T = 25\,^\circ$C. (a) Density extracted from Ref. [41]; the continuous line is $\rho(\phi) = \rho_g\phi + (1-\phi)\rho_w$, with $\rho_g$ and $\rho_w$ the densities of pure glycerol and water, respectively. (b) Mutual diffusion coefficients extracted from Refs. [42–44]; the various symbols correspond to the different references. (c) Activity extracted from Refs. [45–47]. The continous lines in (b) and (c) correspond to Eqs. (31).

since this quantity is difficult to measure precisely. We fit these two quantities according to

$$D(\phi) = 0.6517\phi^2 - 1.6012\phi + 0.9994,$$
$$a(\phi) = (1-\phi)(1 + 0.8714\phi - 0.094\phi^2 + 1.009\phi^3), \quad (31)$$

and we use these formulas to solve numerically the model describing the confined droplet, Eqs. (20)–(22). A similar strategy was adopted by Doumenc *et al.* to model the drying of a solution in a moving meniscus but for polymer solutions [48].

#### 2. Concentration in the confined droplet

We illustrate the case of such water-glycerol mixtures in the confined droplet by solving Eqs. (20)–(22) for several sets of typical parameters $\beta$ and Pe. We set $a_e = 0$ for simplicity, as this parameter can be easily tuned to zero in the experiments [9]. Figure 7 displays two typical cases for droplets at an initial volume fraction $\phi = 0.4$, but for two different $\beta$. $\beta$ corresponds to the ratio of the area of the initial droplet over the area of the wafer, and thus directly tunes the Péclet number Pe (see Sec. II D).

Figure 7 evidences that drying is faster for $\beta = 0.2$, since the final concentration $\phi \approx 1$ is reached at a smaller time compared to $\beta = 0.8$. This is a nontrivial effect as compared to dilute solutions, because one expects that smaller $\beta$ induces slower drying kinetics. Actually, the Péclet number is also small for small $\beta$, and evaporation of the solvent does not induce concentration gradients in the droplet (see Fig. 7, left).

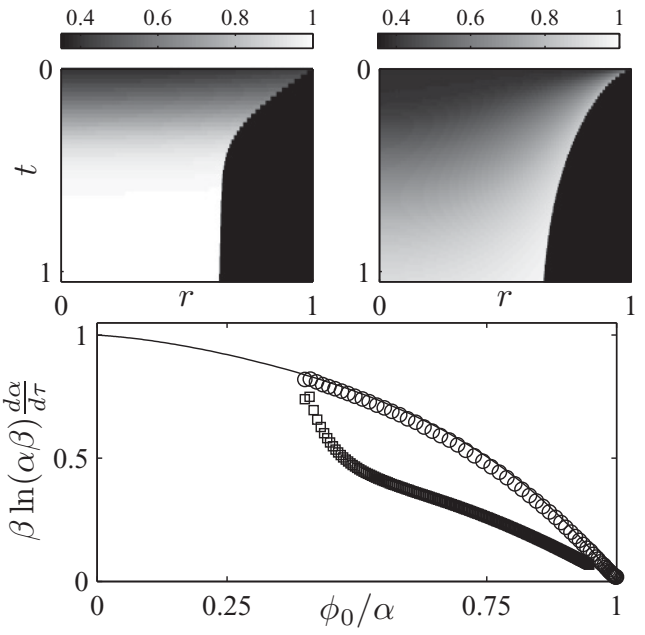


FIG. 7. Space-time plots of the concentration of glycerol in the evaporating droplet. Left: $\beta = 0.2$, Pe $= 0.088$; right: $\beta = 0.8$, Pe $= 1.408$. In both cases, we take into account the variation of activity and of diffusivity Eq. (31), and the glycerol-water mixture is initially at a volume fraction $\phi_0 = 0.4$. Bottom: Estimated activities from the variation of the area of the droplet against the estimated concentration in the droplet $\phi_0/\alpha$ (see text, $\circ \to \beta = 0.2$, $\square \to \beta = 0.8$). The continuous line is the activity of water-glycerol mixture vs $\phi$.

For higher $\beta$, Pe $> 1$, and strong concentration gradients build up in the droplet during drying (Fig. 7, right). In this case, the concentration of glycerol becomes rapidly large at the edge of the drop and creates a *barrier* for evaporation, since the activity decreases with the glycerol concentration [Fig. 6(c)].

Finally, one can extract the activity of mixtures from such drying experiments without measuring the concentration field of solute [9]. Indeed, a precise monitoring of the area of the droplet only permits an estimation of the activity of the mixture, since its evolution [see Eq. (20)] depends on $a(\phi^\star)$, $\phi^\star$ being the solute concentration at the edge of the droplet. For small $\beta$ and thus small Pe numbers, concentration gradients are small in the droplet, and the concentration in the droplet is simply estimated from the measurement of $\alpha$ and the volume conservation $\phi \approx \phi^\star \approx \phi_0/\alpha$. The evolution of the activity during evaporation is then simply calculated using Eq. (20), i.e., $\beta \ln(\beta\alpha)\dot{\alpha} = a(\phi^\star)$. Such measurements lead to a good estimation for $a(\phi)$ in the case of small Pe numbers ($\beta = 0.2$, see Fig. 7) but deviates clearly at higher Péclet numbers ($\beta = 0.8$).

## IV. DISCUSSIONS AND CONCLUSIONS

In this paper we derived a simple model based on classical transport equations that describes both the kinetics of drying and the concentration field of solute in confined evaporating droplets. We also illustrate several experimental cases already explored [9,10], and we provide a simple analytical formula in the case of dilute solutions.

Our simple model may serve as a starting point for more complex investigations, such as surfactant solutions and other colloidal dispersions. We believe that the droplet method combined with analytical tools measuring the concentration field may give new insights in the physics of dense mixtures. This may be an important issue, namely, for charged dispersions and nanoparticles, since dynamical properties such as the collective diffusion coefficient $D(\phi)$ are difficult to measure but important in the context of solidification [4,49,50].

Finally, several improvements may be done to the present model. For instance, it would be simple to add the case of coexisting phases in the droplet, as already done in other similar studies (microevaporation [25] and sedimentation [36]). This may be useful to describe the concentration of surfactants that leads to the formation of organized mesophases [17]. Importantly, a crucial point is to go beyond the assumption of quiescent droplet during evaporation. Indeed, recent experiments on surfactants [17] reveal important hydrodynamic recirculations, probably due to a solutal Marangoni instability. We are working currently on that issue, and our aim is to determine the regimes where droplets stay quiescent during evaporation.

## ACKNOWLEDGMENTS

We acknowledge B. Selva, J. Leng, and H. Bodiguel for useful discussions. We also thank Région Aquitaine, Université Bordeaux-1, Rhodia, and CNRS for funding and support.

[1] R. D. Deegan, M. Balkanski, T. F. Dupont, G. Huber, S. R. Nagel, and T. Witten, Nature (London) **389**, 827 (1997).

[2] A.-M. Cazabat and G. Guéna, Soft Matter **6**, 2591 (2010).

[3] E. R. Dufresne, D. J. Stark, N. A. Greenblatt, J. X. Cheng, J. W. Hutchinson, L. Mahadevan, and D. A. Weitz, Langmuir **22**, 7144 (2006).

[4] L. Goehring, W. J. Clegg, and A. F. Routh, Langmuir **26**, 9269 (2010).

[5] G. Jing, H. Bodiguel, F. Doumenc, E. Sultan, and B. Guerrier, Langmuir **26**, 2288 (2010).

[6] Z. Lin, J. Polym. Sci., Part B **48**, 2552 (2010).

[7] J. Leng, B. Lonetti, P. Tabeling, M. Joanicot, and A. Ajdari, Phys. Rev. Lett. **96**, 084503 (2006).

[8] P. Moreau, J. Dehmoune, J. B. Salmon, and J. Leng, Appl. Phys. Lett. **95**, 033108 (2009).

[9] F. Clément and J. Leng, Langmuir **20**, 6538 (2004).

[10] J. Leng, Phys. Rev. E **82**, 021405 (2010).

[11] L. Pauchard, M. Mermet-Guyennet, and F. Giorgiutti-Dauphiné, Chem. Eng. Proc. **50**, 483 (2011).

[12] J. Leng (private communication).

[13] W. D. Ristenpart, P. G. Kim, C. Domingues, J. Wan, and H. A. Stone, Phys. Rev. Lett. **99**, 234502 (2007).

[14] H. Hu and R. G. Larson, Langmuir **21**, 3972 (2005).

[15] V. Ha and C. Lai, Int. J. Heat Mass Transf. **45**, 5143 (2002).

[16] G. Toussaint, H. Bodiguel, F. Doumenc, B. Guerrier, and C. Allain, Int. J. Heat Mass Transf. **51**, 4228 (2008).

[17] L. Daubersies, J.-B. Salmon, and J. Leng (2011) (unpublished).

[18] E. L. Cussler, *Diffusion: Mass Transfer in Fluid Systems* (Cambridge University Press, Cambridge, UK, 1997).

[19] B. R. Bird, E. W. Stewart, and E. N. Lightfoot, *Transport Phenomena* (Wiley, New York, 2002).

[20] F. P. Incropera, D. D. Dewitt, T. D. Bergman, and A. S. Lavine, *Fundamentals of Heat and Mass Transfer* (Wiley, New York, 2007).

[21] D. D. Joseph, A. Huang, and H. Hu, Physica D **97**, 104 (1996).

[22] W. B. Russel, D. A. Saville, and W. R. Schowalter, *Colloidal Dispersions* (Cambridge University Press, Cambridge, UK, 1989).

[23] G. Nägele, Phys. Rep. **272**, 215 (1996).

[24] J. C. Slattery, *Advanced Transport Phenomena* (Cambridge University Press, Cambridge, UK, 1999).

[25] M. Schindler and A. Ajdari, Eur. Phys. J. E **28**, 27 (2009).

[26] S. S. Peppin, J. A. Elliott, and M. G. Worster, Phys. Fluids **17**, 053301 (2005).

[27] W. Press, B. Flannery, S. Teukolsky, and W. T. Vetterling, *Numerical Recipes in C* (Cambridge University Press, Cambridge, UK, 1992).

[28] P. N. Pusey and W. van Megen, Nature (London) **320**, 340 (1986).

[29] T. P. Bigioni, X. M. Lin, T. T. Nguyen, E. I. Corwin, T. A. Witten, and H. M. Jaeger, Nat. Mater. **5**, 265 (2006).

[30] Strictly speaking, the activity should a priori vanish approaching the maximal packing fraction as the osmotic compressibility diverges. Actually, if one takes the formula of $Z(\phi)$ given later in the text and $v_m/v_c \approx 510^{-9}$, this effect occurs only for $\phi > \phi_g - 10^{-8}$, far from the validity of the model. Moreover, evaporation rates never drop to zero, and solvent still evaporates from such packed assembly even at the random close packing fraction. Indeed, air-water menisci can form inside the *porous* material as soon as the pore radii are larger than the Kelvin radius [3], and water still evaporates until the colloidal assembly is left completely dried.

[31] W. R. Bowen, Y. Liang, and P. M. Williams, Chem. Eng. Sci. **55**, 2359 (2000).

[32] J. L. Harland and W. van Megen, Phys. Rev. E **55**, 3054 (1997).

[33] S. S. Peppin, J. A. Elliott, and M. G. Worster, J. Fluid Mech. **554**, 147 (2006).

[34] S. E. Phan, W. B. Russel, Z. Cheng, J. Zhu, P. M. Chaikin, J. H. Dunsmuir, and R. H. Ottewill, Phys. Rev. E **54**, 6633 (1996).

[35] L. V. Woodcock, Ann. NY Acad. Sci. **371**, 274 (1981).

[36] K. E. Davis and W. B. Russel, Phys. Fluids **1**, 82 (1989).

[37] B. J. Ackerson, S. E. Paulin, B. Johnson, W. van Megen, and S. Underwood, Phys. Rev. E **59**, 6903 (1999).

[38] J. Happel and H. Brenner, *Low Reynolds Number Hydrodynamics* (Kluwer Academic Publishers, Dordrecht, The Netherlands, 1991).

[39] A. F. Routh and W. B. Zimmerman, Chem. Eng. Sci. **59**, 2961 (2004).

[40] R. Zheng, Eur. Phys. J. E **29**, 205 (2009).

[41] D. R. Lide, *Handbook of Chemistry and Physics* (CRC Press, Boca Raton, FL, 2004-2005).

[42] G. D'Errico, O. Ortona, F. Capuano, and V. Vitagliano, J. Chem. Eng. Data **49**, 1665 (2004).

[43] N. Rashidnia and R. Balasubramaniam, Exp. Fluids **36**, 619 (2004).

[44] G. Ternström, A. Sjöstrand, G. Aly, and A. Jernqvist, J. Chem. Eng. Data **41**, 876 (1996).

[45] A. N. Kirgintsev and A. V. Luk'yanov, Russ. Chem. Bull. **11**, 1393 (1962).

[46] L. Ninni, M. S. Camargo, and A. J. A. Meirelles, J. Chem. Eng. Data **45**, 654 (2000).

[47] C. Marcolli and T. Peter, Atmos. Chem. Phys. **5**, 1545 (2005).

[48] F. Doumenc and B. Guerrier, Langmuir **26**, 13959 (2010).

[49] A. Sarkar and M. S. Tirumkudulu, Langmuir **25**, 4945 (2009).

[50] A. Merlin, J. Angly, L. Daubersies, C. Madeira, S. Schöder, J. Leng, and J. B. Salmon, Eur. Phys. J. E **34**, 58 (2011).